Distinct Solid-Electrolyte-Interphases on Sn (100) and (001) Electrodes Studied by Soft X-Ray Spectroscopy

ARTICLE *in* ADVANCED MATERIALS · JUNE 2014

Impact Factor: 17.49 · DOI: 10.1002/admi.201300115

9 AUTHORS, INCLUDING:

Altaf Karim
COMSATS Institute of Information Technol…
35 PUBLICATIONS **214** CITATIONS
SEE PROFILE

Jarosław Syzdek
Warsaw University of Technology
19 PUBLICATIONS **144** CITATIONS
SEE PROFILE

Kristin Aslaug Persson
University of California, Berkeley
90 PUBLICATIONS **1,790** CITATIONS
SEE PROFILE

Robert Kostecki
Lawrence Berkeley National Laboratory
133 PUBLICATIONS **3,808** CITATIONS
SEE PROFILE

Distinct Solid-Electrolyte-Interphases on Sn (100) and (001) Electrodes Studied by Soft X-ray Spectroscopy

*Ruimin Qiao, Ivan T. Lucas, Altaf Karim, Jaroslaw Syzdek, Xiaosong Liu, Wei Chen, Kristin Persson, Robert Kostecki, Wanli Yang**

Dr. R. Qiao, Dr. X. Liu, Dr. W. Yang
Advanced Light Source, Lawrence Berkeley National Laboratory
Berkeley, CA 94720, USA
E-mail: wlyang@lbl.gov
Dr. I. T. Lucas, Dr. A. Karim, Dr. J. Syzdek, Dr. W. Chen, Dr. K. Persson, Dr. R. Kostecki
Environmental Energy Technologies Division, Lawrence Berkeley National Laboratory
Berkeley, CA 94720, USA
Dr. I. T. Lucas
UPMC Univ Paris 06, Sorbonne Universités, UPR 15, LISE, F-75252, Paris, France
Dr. A. Karim
Department of Physics, COMSATS Institute of Information Technology, Islamabad, Pakistan

Keywords: solid electrolyte interphases, Sn electrodes, lithium ion batteries, soft x-ray absorption spectroscopy

Soft x-ray absorption spectroscopy at different probe depth was employed to characterize the solid electrolyte interphases (SEIs) formed on β-Sn single crystals with two different surface orientations. Based on comparative studies of C-*K*, O-*K*, and F-*K* absorption spectra between the SEIs and reference samples, SEI on Sn (100) mainly consists of porous Li_2CO_3 species with electrolyte uptake, while SEI on Sn (001) is essentially a layer of LiF and organic molecules, with a small amount of $–CO_3$ and electrolyte buried inside. Theoretical calculation suggests that Sn (001) surface is more reactive than (100), especially after air exposure. The reactive (001) surface facilitates the decomposition of $LiPF_6$ to form a LiF layer. In contrast, SEI on (100) surface is predominately from the typical decomposition of carbonate-based electrolyte. While the LiF passivates Sn (001) electrode after one cycle, the porous carbonate layer on (100) surface does not prevent further decomposition of electrolyte after many cycles. This leads to drastically different electrochemical behavior and morphology of the two surfaces. The result is a direct proof that different surfaces of active materials could strongly

impact the SEI formation on electrodes even with the same electrolyte. Such effect could lead to dramatically different electrochemical performance.

1. Introduction

The development of high-energy batteries requires both fundamental understanding and practical development of electrolytes that display large electrochemical windows and form high quality solid electrolyte interphases (SEIs) on the electrode surfaces. The stability and passivating capability of SEI is critical for the performance of lithium-ion batteries.[1, 2] The majority of the SEI studies are performed on anode surfaces, mainly due to the fact that many anode materials exhibit electrochemical potentials well below the reduction potential of the electrolyte species.[3-5] In previous works, SEIs with different morphology and composition have been detected with the same type of electrolyte on different electrode materials[6-9] or on different electrode surfaces.[10, 11] These results indicate that the electrode materials often play important roles in SEI formation. The same type of effect has also been observed on $LiMn_2O_4$ cathodes with different surface orientations.[12] Clarifying the impact of electrode active materials on the formation, composition and stability of the SEIs is an important step towards understanding and control of the SEIs in batteries, which remains one of the most challenging and critical issues in battery technology.[4, 5, 13]

Tin has been proposed as an alternative lithium storage anode material to replace graphite. It has attracted significant attention over the past several years, because it offers a large specific capacity (993mAh g^{-1} for $Li_{22}Sn_5$)[14, 15] as compared to graphite (372mAh g^{-1} for LiC_6).[16] However, compared with the relatively stable SEI formed on graphite anode in commonly used EC-based electrolytes, the SEI layer that develops on polycrystalline Sn anode is highly unstable.[17] The constant reformation of the SEI upon cycling consumes lithium and affects the cyclability of the battery, which has severely impeded the development of Sn anodes for lithium-ion battery applications.[15, 17-25] Therefore, clarifying the mechanism

of electrolyte degradation and SEI formation on Sn anodes are of both fundamental and practical importance.

In this work, we perform synchrotron based soft x-ray absorption spectroscopy (sXAS) and energy-dispersive x-ray spectroscopy (EDX) on two single crystal Sn electrodes, β-Sn (100) and (001). In addition, density functional theory (DFT) calculations are performed to elucidate the surface reactivity. SEIs are formed on the Sn surfaces by cycling in 1 mol L^{-1} $LiPF_6$, ethylene carbonate/diethyl carbonate (EC:DEC, 1:2, w:w) electrolyte. A previous study shows that the SEI formed on the β-Sn (100) and (001) electrode surfaces, in an EC-based electrolyte, exhibit different morphology as well as electrochemical behavior.[11] Through sXAS and EDX studies, we now reach a comprehensive understanding of both the chemical composition and the formation mechanism of SEIs on the two different Sn surfaces. Our combined spectroscopic and theoretical studies suggest that the oxidized Sn (001) surface is more chemically reactive than the (100) surface, which leads to the decomposition of $LiPF_6$ to form a layer of LiF. The formation of the LiF prevents further decomposition of the organic solvent in electrolyte after one cycle. In contrast, the SEI on the Sn (100) surface is Li_2CO_3 based, and is highly porous and unstable. We show that the different SEI formation mechanisms are responsible for the morphological and electrochemical properties of the SEIs on Sn (100) and (001) surfaces.

2. Results

β-Sn (100) and (001) single crystal discs (20 mm diameter, 3mm thick) were purchased from Leico Industries, Inc. Their surface orientation was verified by x-ray Laue diffraction (**Figure 1**). Both Sn single crystal electrodes were polished in air to a mirror-like finish, rinsed with water and acetone, dried under N_2 flow, heated at 80 °C under vacuum for 4 h, and transferred to a He-filled glove box (VAC, O_2: <0.1 ppm, H_2O: <0.5 ppm). Oxidation on the single crystal surfaces can be clearly detected by sXAS (Figure 1c).[24, 26] As elaborated later,

this surface oxidation layer plays an important role in the SEI formation on different Sn surfaces. SEI formation on surfaces prepared under inert atmosphere exhibit different phenomena but is outside the scope of this work. For deciphering the composition of the SEI, we also performed sXAS on a series of relevant compounds, Li_2CO_3, Li_2O_2, Li_2O, LiOH, SnO_2, $LiPF_6$, LiF, SnF_2 and SnF_4 (Sigma-Aldrich).

To maximize consistency and allow comparison with earlier works, the same cycling procedure as described in the previous report has been implemented to induce the SEI formation on the Sn single crystal electrodes.[11] Compared with commonly used techniques for SEI characterizations, for example, Fourier transform infrared spectroscopy (FTIR)[22-24, 27, 28] and X-ray photoelectron spectroscopy (XPS),[10, 27] sXAS is arguably the most sensitive probe of the chemical bonds and electronic states with elemental sensitivity.[29-31] sXAS provides fingerprints of the chemical species and bonds through the electron excitation process, and is sensitive to all the compounds involved in SEI formation, including LiF that are FTIR inactive. In addition, the two detecting modes of sXAS, total electron yield (TEY) and total fluorescence yield (TFY), supply surface-sensitive and bulk-sensitive information respectively. Data presented here are collected in both modes simultaneously, with probe depth of less than 10nm for TEY and more than 100nm for TFY.

Figure 2a-b show the cyclic voltammetry (CV) cycling of the β-Sn (100) and (001) single crystal electrodes in 1mol L^{-1} $LiPF_6$, EC:DEC (1:2, w:w) electrolyte. In the first cycle, β-Sn (100) electrode exhibits a large and broad peak centered on 0.9 V that reaches -2150 μA cm^{-2}, while β-Sn (001) displays a sharp peak of -70 μA cm^{-2} at 1.4V and a small shoulder at 1.3V. The total charge consumed in the first cycle for β-Sn (100) is roughly 50 times larger than that for β-Sn (001). During the second cycle, while the current density drops dramatically for the β-Sn (001), it remains high for β-Sn (100), indicating the (100) surface is not passivated. The different potentials of the current peak (0.95 vs 1.4 V) suggest distinct electrolyte reduction reaction pathways on β-Sn (100) and (001) surfaces. The difference in

morphology of SEIs on Sn (100) and (001) electrodes is revealed by SEM in Figure 2c-d. A porous and non-uniform surface layer is visible on Sn (100), contrasting the compact and dense film on Sn (001). Both the electrochemical and morphological results are consistent with, and have been discussed in, the previous report.[11]

To obtain the elemental composition of the SEIs on the two crystal surfaces, EDX spectroscopy is performed and the results are presented in Figure 2e-f. Some variations on elemental concentration are observed at different spots on the Sn (100) surface; however, the predominance of O and P is evident on the Sn (100) surface. In contrast, only small amount of O, but high concentration of F was detected on Sn (001). To experimentally clarify the chemical species of the SEIs, and to elucidate the electrolyte reaction pathways, we perform C-*K*, O-*K*, and F-*K* sXAS experiments on the two SEIs.

Figure 3 shows the C *K*-edge sXAS spectra of the SEIs on Sn (100) and (001) single crystal electrodes, and reference spectra collected on Li_2CO_3. The SEIs on Sn (100) (red) and (001) (blue) display dramatically different sXAS profiles. The most significant C-*K* absorption feature for Sn (100) sits at 290.3eV, which is assigned to electron transitions from the C 1*s* core level to the unoccupied (C=O) π^* orbital.[32] The CO_3^{2-} functional group has a strong resonance at this particular energy, and it has been found that C-*K* sXAS of different carbonate species exhibit very different relative intensity of this feature.[33] Therefore, the high similarity of the spectra collected on the (100) surface and Li_2CO_3 indicates that Li_2CO_3 species are the dominant component of SEI on the Sn (100) surface. Formation of Li_2CO_3 based SEI is typically due to the decomposition of EC:DEC electrolyte. Additionally, metastable and poorly passivating compounds like ROLi and $ROCO_2Li$ may also convert to Li_2CO_3.[34]

In sharp contrast, for Sn (001), the intensity of the $\pi^*_{(C=O)}$ peak is almost negligible in the surface-sensitive TEY spectrum, and slightly higher in the bulk-sensitive TFY. Therefore, only a limited amount of $-CO_3$ is formed on Sn (001) at the early stage of the SEI formation,

which is only detected by TFY with deeper probe depth. The very small amount of $-CO_3$ species are quickly covered by other compounds formed in the subsequent electrochemical process, and the sXAS through surface-sensitive TEY does not detect a strong signal at 290.3 eV.

To further specify the non-CO_3 species in the SEI formed on the Sn (001) surface, we measured sXAS at O-*K* and F-*K* edges. Also, we tested possible decomposition products of the carbonate solvent (EC/DEC) in electrolyte, such as Li_2O, Li_2CO_3, polyolephines and semicarbonates.[4] Based on the O-*K* spectra (**Figure 4**), both TEY and TFY spectra of the SEIs on Sn (100) resemble that of Li_2CO_3, which features the sharp O 1*s*- $\pi^*_{(C=O)}$ absorption peaks at 534eV.[35] The result confirms again that Li_2CO_3 is the dominant SEI component on Sn (100) electrode. For Sn (001), the contrast between O-*K* TEY and TFY spectra confirms again that there are finite amount of -CO_3 sitting deep in the SEI, which is detected only by the bulk-sensitive TFY. Moreover, the comparison of the O-*K* sXAS spectra between SEIs and reference samples, including Li_2O_2, Li_2O and LiOH, show that none of these reference compounds are detectable in both SEIs samples.

It is worthy to note that the difference of O-*K* spectra collected on the two SEI samples are not only on the fingerprinting $-CO_3$ peak at 534 eV. In the (001) SEI sample, a broad hump around 537 eV is seen especially with TEY data, which suggests the existence of other SEI components like organic molecules in the SEI. Additionally, the absorption features below 290eV shown on the C-*K* spectra (Figure 3) can be related to electron transitions from the C 1*s* core level to the unoccupied (C=C) π^* orbital and (C-H) σ^* orbital, respectively.[32] Such features from C=C and C-H bonds generally manifest in organic molecules.[33] Therefore, the overall similar lineshape of both O-*K* and C-*K* spectra of the (100) SEI and Li_2CO_3 indicates negligible amount of organic carbon species in the (100) SEI. However, for (001) SEI, the C=C and C-H features in C-*K* spectra (Figure 3), and the hump around 537 eV in O-K spectra (Figure 4), indicate the existence of other organic molecules. As a matter of fact, it has been

suggested that organic molecules, such as lithium oxalate, lithium carboxylate, lithium alkoxide, lithium alkyl mono- and dicarbonates, are compounds in the SEI.[4, 36, 37]

Finally, we are able to determine the dominating compound in the (001) SEI through F-K sXAS experiments. As shown in **Figure 5**, no tin fluoride, SnF_4 or SnF_2, is observed in the SEI samples. Compared with that of the (001) surface, the F-*K* absorption profile of the (100) surface shows much higher intensity near the absorption edge and has more broadened features in the whole region. Such F-*K* TEY and TFY spectra of SEI on Sn (100) are identical to that of $LiPF_6$. This could be easily understood by considering the electrolyte uptake by a porous SEI layer on Sn (001) surface, so the $LiPF_6$ salt in electrolyte is detected in the sample.

Surprisingly, the F-*K* TEY spectrum of (001) SEI resembles that of LiF. The TFY spectrum shows slightly higher $LiPF_6$ feature near the absorption edge. The small contrast between TEY and TFY data suggests a small amount of $LiPF_6$ exist inside the (001) SEI, which is detected by bulk-sensitive TFY. This is again consistent with the existence of finite amount of -CO_3 inside the bulk of SEI, as discussed above for understanding the C-*K* spectra. Therefore, the dominating chemical component of the SEI formed on Sn (001) surface is LiF (Figure 5b).

3. Discussion

The combined C, O, and F *K*-edge sXAS analysis clearly show that the SEI formed on Sn (100) surface mainly consists of porous Li_2CO_3 species with electrolyte uptake, while the SEI on Sn (001) is essentially a layer of LiF, with organic molecules, a small amount of –CO_3 and electrolyte buried inside. In the perspective of elements, this conclusion is in good agreement with the EDX results, which show mainly O (from -CO_3) and P (from electrolyte) elements for (100) SEI, but F for (001) SEI (Figure 2).

The distinct SEIs formed on Sn (001) and (100) surfaces are also consistent with the different electrochemical data. The different reaction potentials (Figure 2) originate from the

formation of different species, i.e., Li_2CO_3 from EC:DEC for Sn (100) and LiF from $LiPF_6$ for Sn (001). Our explaination is qualitatively supported by previous findings that the reduction of the carbonate solvent (~1-1.5 V vs Li/Li^+)[38] occurs at lower potential than the salt $LiPF_6$ (1.5-2.5 V vs Li/Li^+)[39, 40]. The LiF based layer effectively passivates the Sn (001) surface and serves as a stable interphase to prevent further electrolyte reduction, so the charge consumption is greatly reduced after only one cycle (Figure 2b). On the contrary, the highly porous Li_2CO_3 based layer on Sn (100) surface leads to large amount of electrolyte uptake. This is evidenced by the PF_6^- group observed in F-*K* XAS (Figure 5) and the strong P element peak in EDX (Figure 2). The absorbed electrolyte in SEI remains contacting with the Sn (100) surface, which keeps the electrolyte decomposition active even after several cycles (Figure 2a). Besides the stability issue, it has been shown by Aurbach[41] that SEI films containing larger fractions of LiF compared to the carbonates tend to show high impedance and poor lithium mobility. We emphasize that no lithiation/delithiation of the single-crystal Sn is performed, so we discuss here only the stability, not the functionality, of the SEIs formed on different Sn facets. Thus, our study is focused on understanding the formation mechanism and stability of SEIs, as well as their strong dependence on the underlying surface facet chemistry.

The radically different chemical compositions and electrochemical properties of SEIs formed on β-Sn(100) and Sn(001) electrodes provide us a model system to understand the mechanism of the SEI formation on Sn. As shown in **Table 1**, we performed first principle calculations on the surface energies of (100) and (001) β-Sn with three different surface termination.[42] We used a slab model for the surface energy calculations, where the top two layers of both sides were fully relaxed and the four central layers were kept at the bulk positions. The surface energies were calculated by $E_{surface} = (E_{slab} - nE_{bulk})/2a$, where a is the surface area. The calculations show that β-Sn (001) has higher surface energy than (100), which suggests stronger chemical reactivity of (001) surface and is intuitively consistent with

the larger number of unsaturated bonds/unit area on the (001) surface. In order to mimic our experimental β-Sn single crystal surfaces, which are polished in air with a water-based paste, additional calculations are performed on tetragonal Sn with O and H connected to the non-coordinated Sn atomes on the surfaces. On such O- and (H,O)- terminated β-Sn surfaces, the difference in surface energy is much enhanced (Table 1). As the best representative of our experimental condition, the (H, O)-terminated β-Sn (001) surface shows a 63% increase on surface energy (5.01 J/m^2) compared with that of (100) surface (3.08 J/m^2), indicating much higher chemical reactivity of the (H,O)- terminated (001) surface.

Although a functional SEI is typically formed by solvent decomposition and $–CO_3$ deposition, the porousness of the Li_2CO_3 based SEI on the (100) surface cannot protect the electrolyte from further reactions. The (001) surface, however, is much more reactive, and facilitates the decomposition of $LiPF_6$ salt into LiF to form a dense and effective passivating layer. Because no Sn- based species, e.g., SnO_2, SnF_2, and SnF_4, are found in SEIs, even with the bulk-sensitive TFY sXAS (Figure 4 and 5), Sn electrodes likely play a catalytic role of the SEI formation. Additionally, $LiPF_6$ decomposition takes place at a higher potential than that for solvent. Formation of LiF layer on the (001) surface is thus before the $–CO_3$ formation. The dense LiF layer then retards the further solvent decomposition at lower potential, leading to very limited amount of $–CO_3$ species in the SEI on the (001) surface.

With the clarified SEI formation mechanism, we further extend our theoretical calculations to other low index surfaces of β-Sn to investigate its equilibrium particle morphology (**Table 2**). We calculated the surface energies and performed Wulff construction using the calculated values (**Figure 6**). Wulff construction is a powerful tool to determine the equilibrium shape and preferred surfaces of a crystal.[43] The Wulff shape of β-Sn indicates that Sn particles formed under thermodynamic equilibirum conditions would have dominant (100) surfaces compared to the (001). Due to the existence of low energy (101) surface, the (001) surface does not manifest as a facet in the Wulff shape of β-Sn. The predominant (100)

surface in the equilibrium shape of β-Sn crystal implies the fundamental challenge of Sn particles as battery anodes. Therefore, novel material synthesis and/or surface treatment are critical to avoid the SEI stability issue for utilizing β-Sn as battery anodes.

4. Conclusion

We performed sXAS, EDX, SEM, electrochemical cycling, and DFT calculations of the SEIs formed on β-Sn (100) and (001) single crystal electrodes with $LiPF_6$, EC:DEC electrolyte. The combined studies show self-consistent results to reveal the distinct SEI formation mechanism on the two electrode surfaces. The sXAS technique with different probe depth, through TEY and TFY channels, clearly shows that Li_2CO_3 and LiF are the primary compositions of the SEIs on Sn (100) and (001), respectively. The SEI formed on Sn (100) surface is a porous and unstable layer consuming a high degree of electrolyte solvent, while LiF forms a stable passivating layer on the Sn (001) surface with organic molecules and small amount of $–CO_3$ inside. These findings are consistent with the morphology, elemental distribution, and electrochemical tests, and clarify the chemical components and reaction pathways of the SEI formation on the two different Sn crystal surfaces.

Additionally, DFT calculations suggest the (001) surface is more reactive than (100), and preferentially decomposes $LiPF_6$ to form a passivating LiF layer. Our work provides direct evidences that the surface facets of β-Sn electrodes play critical roles in the process of electrolyte decomposition and SEI formation. While LiF is unlikely to form a functional lithiation/delithiation SEI due to presumed lower Li mobility, our results show how electrode materials can be tailored to specific SEI formation by promoting certain facets in the synthesis process. The different formation mechanism revealed here provides useful information for understanding the critical SEI issues on Sn electrodes, and may lead to possibilities for practical optimizations.

5. Experimental Section

Sample preparation and electrochemical test: The SEI formation and CV tests are performed in a three electrode cell equipped with Li-foil counter and reference electrodes and filled with 1M $LiPF_6$, EC:DEC (1:2, w:w) electrolyte (Novolyte Technologies, Inc.). The CV cycling of the electrodes at 1mV s^{-1} was limited to 0.8-2.5 V to avoid any lithiation of the electrode and associated volume expansion. After cycling, both crystals were rinsed with DEC to remove the excess of electrolyte. Cycled Sn samples and reference samples were transferred to the XAS chambers through Ar filled glove bags or special transfer kit to avoid air exposure.

Soft X-ray Spectroscopy: sXAS measurements of C, O and F *K*-edges were performed at beamline 8. 0. 1 of the Advance Light Source (ALS) at Lawrence Berkeley National Laboratory (LBNL). The undulator and spherical grating monochromator supply a linearly polarized photon beam with resolving power up to 6000.[44] The energy resolution of sXAS is higher than 0.15 eV in this study. All experiments are performed at room temperature. All the spectra were normalized to the beam flux measured by an upstream gold mesh, which is cleaned through in-vacuum Au evaporation especially for C-*K* and O-*K* sXAS experiments.

X-ray Laue Diffraction and Characterization: X-ray Laue diffraction patterns are collected by a real-time area detector from Multiwire Laboratories Ltd, with hard x-ray source from General Electronic. EDX was carried out on a JEOL 7500 FESEM with a tungsten field emission filament at an accelerating voltage of 15 kV, and with the detector from Oxford instruments.

First Principle Calculations: First principle calculations are carried out using density functional theory implemented in the Vienna *ab initio* simulation package (VASP).[45, 46] The convergences of total energy with respect to the plane wave energy cutoff and k-point sampling were carefully tested. The final series of energies were computed with an energy cutoff of 520 eV and integration using at least 90 k-point sampling over the supercell irreducible Brillouin zone, which was generated by the Monkhorst−Pack scheme. This

scheme was used to ensure that total energy of the system is converged within 5 meV per formula unit. The relaxed bulk structures were taken from the Materials Project[47] and the surface slabs were generated using the algorithm by Wenhao et al.[48] The Wulff shape were generated using the algorithm developed by Zucker et al.[49]

Acknowledgements
We thank Dr. Philip N. Ross, Dr. Stephen J. Harris, Dr. Zhi Liu, and Mr. Victor von Miller for thoughtful discussions. The Advanced Light Source is supported by the Director, Office of Science, Office of Basic Energy Sciences, of the U.S. Department of Energy. This work is also supported by the Assistant Secretary for Energy Efficiency and Renewable Energy, Office of FreedomCAR and Vehicle Technologies of the U.S. Department of Energy. Both are under Contract No. DE-AC02-05CH11231.

Received: ((will be filled in by the editorial staff))
Revised: ((will be filled in by the editorial staff))
Published online: ((will be filled in by the editorial staff))

[1] J. B. Goodenough, Y. Kim, Chem. Mater. **2009**, 22, 587.

[2] K. Xu, Chem. Rev. **2004**, 104, 4303.

[3] R. Fong, U. von Sacken, J. R. Dahn, J. Electrochem. Soc. **1990**, 137, 2009.

[4] P. B. Balbuena, Y. Wang, *Lithium-ion batteries: Solid-electrolyte interphase*, Imperial College Press, London, UK **2004**.

[5] P. Verma, P. Maire, P. Novák, Electrochim. Acta **2010**, 55, 6332.

[6] M. R. Wagner, P. R. Raimann, A. Trifonova, K.-C. Moeller, J. O. Besenhard, M. Winter, Electrochem. Solid-State Lett. **2004**, 7, A201.

[7] D. Aurbach, B. Markovsky, A. Shechter, Y. Ein-Eli, H. Cohen, J. Electrochem. Soc. **1996**, 143, 3809.

[8] N. Tamura, R. Ohshita, M. Fujimoto, S. Fujitani, M. Kamino, I. Yonezu, J. Power Sources **2002**, 107, 48.

[9] D. Aurbach, E. Zinigrad, Y. Cohen, H. Teller, Solid State Ionics **2002**, 148, 405.

[10] E. Peled, D. Bar Tow, A. Merson, A. Gladkich, L. Burstein, D. Golodnitsky, J. Power Sources **2001**, 97–98, 52.

[11] I. T. Lucas, J. Syzdek, R. Kostecki, Electrochem. Commun. **2011**, 13, 1271.

[12] M. Hirayama, H. Ido, K. Kim, W. Cho, K. Tamura, J. i. Mizuki, R. Kanno, J. Am. Chem. Soc. **2010**, 132, 15268.

[13] V. Zorba, J. Syzdek, X. Mao, R. E. Russo, R. Kostecki, Appl. Phys. Lett. **2012**, 100, 234101.

[14] I. A. Courtney, J. R. Dahn, J. Electrochem. Soc. **1997**, 144, 2045.

[15] M. Winter, J. O. Besenhard, Electrochim. Acta **1999**, 45, 31.

[16] J. R. Dahn, T. Zheng, Y. Liu, J. S. Xue, Science **1995**, 270, 590.

[17] I. T. Lucas, E. Pollak, R. Kostecki, Electrochem. Commun. **2009**, 11, 2157.

[18] R. A. Huggins, Solid State Ionics **1998**, 113–115, 57.

[19] S. D. Beattie, T. Hatchard, A. Bonakdarpour, K. C. Hewitt, J. R. Dahn, J. Electrochem. Soc. **2003**, 150, A701.

[20] S. Yang, P. Y. Zavalij, M. S. Whittingham, Electrochem. Commun. **2003**, 5, 587.

[21] M. Inaba, T. Uno, A. Tasaka, J. Power Sources **2005**, 146, 473.

[22] J.-T. Li, S.-R. Chen, X.-Y. Fan, L. Huang, S.-G. Sun, Langmuir **2007**, 23, 13174.

[23] S. W. Song, S. W. Baek, Electrochim. Acta **2009**, 54, 1312.

[24] J.-S. Bridel, S. Grugeon, S. Laruelle, J. Hassoun, P. Reale, B. Scrosati, J.-M. Tarascon, J. Power Sources **2010**, 195, 2036.

[25] G. Derrien, J. Hassoun, S. Panero, B. Scrosati, Adv. Mater. **2007**, 19, 2336.

[26] S. O. Kucheyev, T. F. Baumann, P. A. Sterne, Y. M. Wang, T. van Buuren, A. V. Hamza, L. J. Terminello, T. M. Willey, Phys. Rev. B **2005**, 72, 035404.

[27] S. Park, J. H. Ryu, S. M. Oh, J. Electrochem. Soc. **2011**, 158, A498.

[28] D. Aurbach, M. Moshkovich, Y. Cohen, A. Schechter, Langmuir **1999**, 15, 2947.

[29] F. de Groot, A. Kotani, *Core Level Spectroscopy of Solids*, CRC Press Taylor & Francis Group, Boca Raton, FL, USA **2008**.

[30] C. Delacourt, A. Kwong, X. Liu, R. Qiao, W. L. Yang, P. Lu, S. J. Harris, V. Srinivasan, J. Electrochem. Soc. **2013**, 160, A1099.

[31] W. Yang, X. Liu, R. Qiao, P. Olalde-Velasco, J. D. Spear, L. Roseguo, J. X. Pepper, Y.-d. Chuang, J. D. Denlinger, Z. Hussain, J. Electron Spectrosc. Relat. Phenom. **2013**, 190, 64.

[32] J. Stöhr, *NEXAFS Spectroscopy*, Springer, Berlin, Germany **1992**.

[33] A. Augustsson, M. Herstedt, J. H. Guo, K. Edstrom, G. V. Zhuang, J. P. N. Ross, J. E. Rubensson, J. Nordgren, Phys. Chem. Chem. Phys. **2004**, 6, 4185.

[34] P. Verma, P. Maire, P. Novak, Electrochim. Acta **2010**, 55, 6332.

[35] R. Qiao, Y.-D. Chuang, S. Yan, W. Yang, PLoS One **2012**, 7, e49182.

[36] G. V. Zhuang, P. N. Ross, Electrochem. Solid-State Lett. **2003**, 6, A136.

[37] K. Xu, G. V. Zhuang, J. L. Allen, U. Lee, S. S. Zhang, P. N. Ross, T. R. Jow, J. Phys. Chem. B **2006**, 110, 7708.

[38] X. Zhang, R. Kostecki, T. J. Richardson, J. K. Pugh, P. N. Ross, J. Electrochem. Soc. **2001**, 148, A1341.

[39] J. S. Gnanaraj, M. D. Levi, Y. Gofer, D. Aurbach, M. Schmidt, J. Electrochem. Soc. **2003**, 150, A445.

[40] D. Aurbach, A. Zaban, J. Electroanal. Chem. **1995**, 393, 43.

[41] D. Aurbach, I. Weissman, A. Zaban, O. Chusid, Electrochim. Acta **1994**, 39, 51.

[42] B. Hammer, J. K. Nørskov, in *Adv. Catal.*, Vol. Volume 45 (Ed: H. K. Bruce C. Gates), Academic Press, **2000**, 71.

[43] E. Ringe, R. P. Van Duyne, L. D. Marks, Nano Lett. **2011**, 11, 3399.

[44] J. J. Jia, T. A. Callcott, J. Yurkas, A. W. Ellis, F. J. Himpsel, M. G. Samant, J. Stohr, D. L. Ederer, J. A. Carlisle, E. A. Hudson, L. J. Terminello, D. K. Shuh, R. C. C. Perera, Rev. Sci. Instrum. **1995**, 66, 1394.

[45] H. J. Monkhorst, J. D. Pack, Phys. Rev. B **1976**, 13, 5188.

[46] G. Kresse, J. Furthmüller, Comput. Mater. Sci. **1996**, 6, 15.

[47] A. Jain, S. P. Ong, G. Hautier, W. Chen, W. D. Richards, S. Dacek, S. Cholia, D. Gunter, D. Skinner, G. Ceder, K. A. Persson, APL Materials **2013**, 1, 011002.

[48] W. Sun, G. Ceder, Surf. Sci. **2013**, 617, 53.

[49] R. Zucker, D. Chatain, U. Dahmen, S. Hagège, W. C. Carter, J. Mater. Sci. **2012**, 47, 8290.

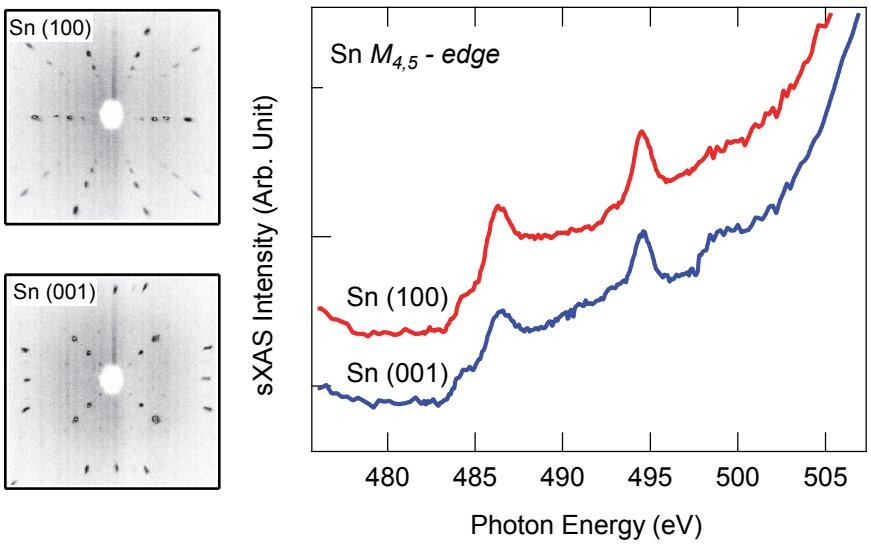

Figure 1. Hard x-ray Laue diffraction patterns (a, b) and Sn *M*-edge soft x-ray absorption spectra (c) collected on Sn single crystals after exposure in air. The leading edge shoulder below 485 eV is from metallic Sn, and the two peaks at higher energies are from surface oxidation that is evident on both surfaces.

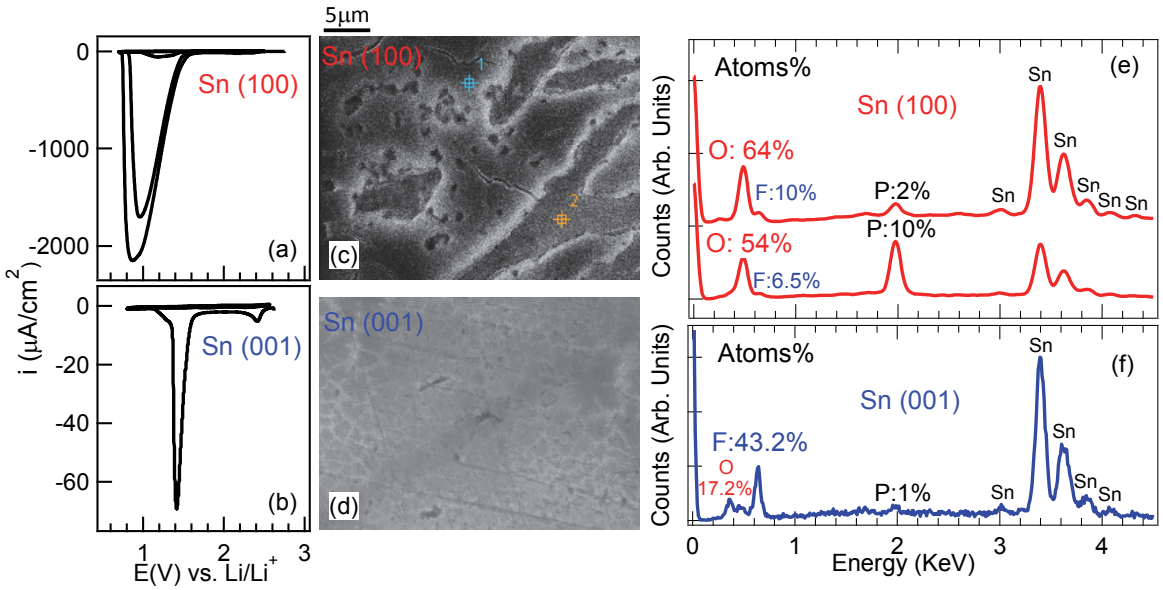

Figure 2. (a, b) CV scans from 2.8 to 0.8 V vs Li/Li$^+$ at 1mV s^{-1} in 1M $LiPF_6$, EC:DEC (1:2, w:w) electrolyte. (c, d) SEM analysis of the SEI morphology on the two single crystal surfaces. (e, f) EDX analysis of the SEI elemental composition. Two spots are measured for the non-uniform SEI formed on Sn (100) surface with some quantitative difference. Data collected on β-Sn (100) are plotted in top panels, and Sn (001) in bottom panels.

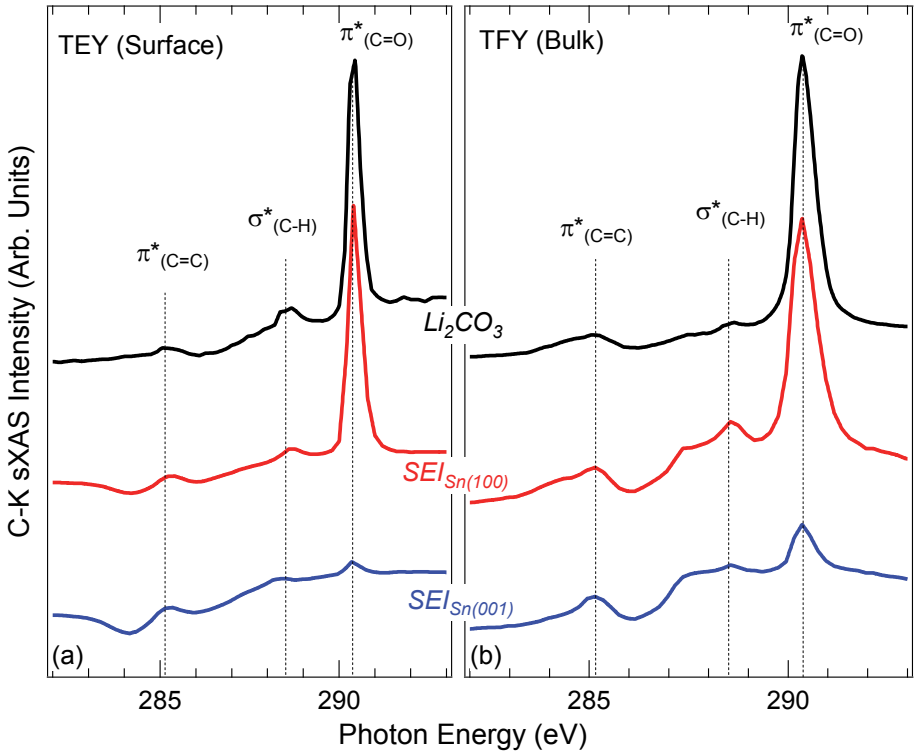

Figure 3. C *K*-edge sXAS spectra of the SEI layers formed on Sn (100) and (001) single crystal electrodes and Li_2CO_3. Results from both the surface-sensitive TEY (a) and bulk-sensitive TFY (b) are plotted.

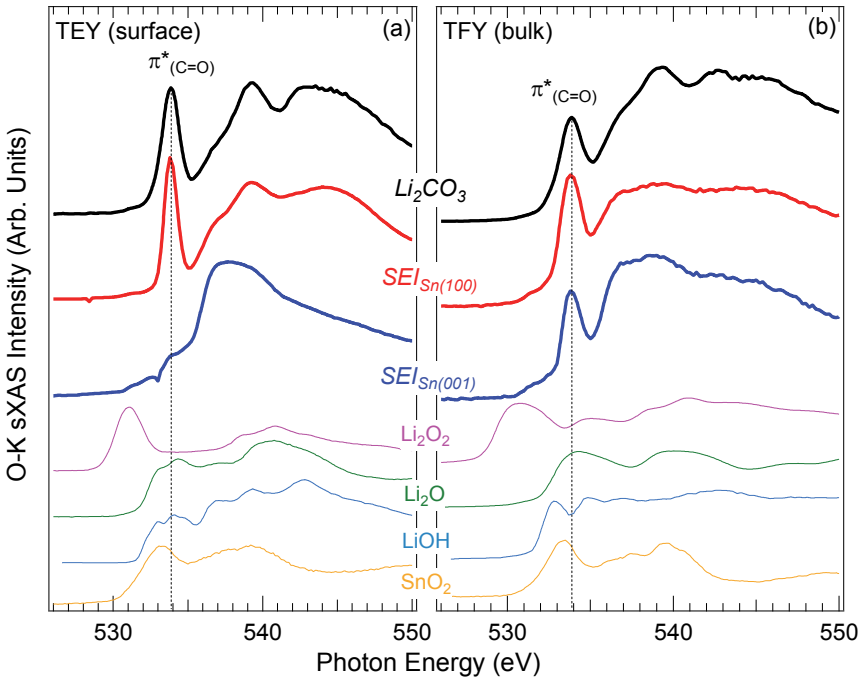

Figure 4. O *K*-edge sXAS spectra of the SEI layers formed on Sn (100) and (001) single crystal electrodes, compared with reference chemicals that could be involved in the SEI formation. Both surface-sensitive TEY (a) and bulk-sensitive TFY (b) data are shown. Li_2O_2, Li_2O, LiOH and SnO_2 are absent on both surfaces.

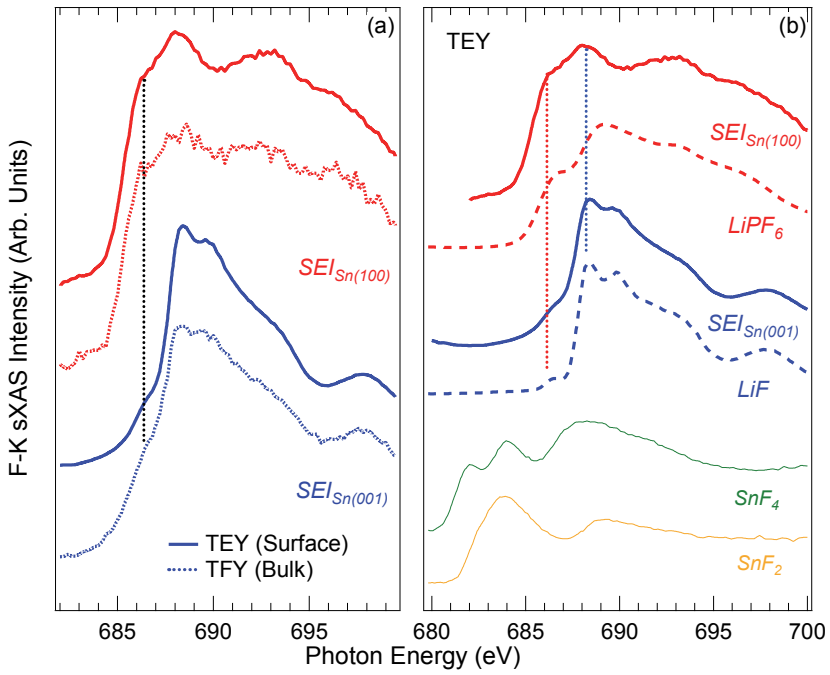

Figure 5. (a) F *K*-edge sXAS spectra of the SEIs formed on Sn (100) and Sn (001) single crystal electrodes. (b) Comparison between the SEI samples and reference compounds, especially LiF and $LiPF_6$. While (100) SEI contains $LiPF_6$ from the Li salt in electrolyte, (001) SEI is dominated by LiF.

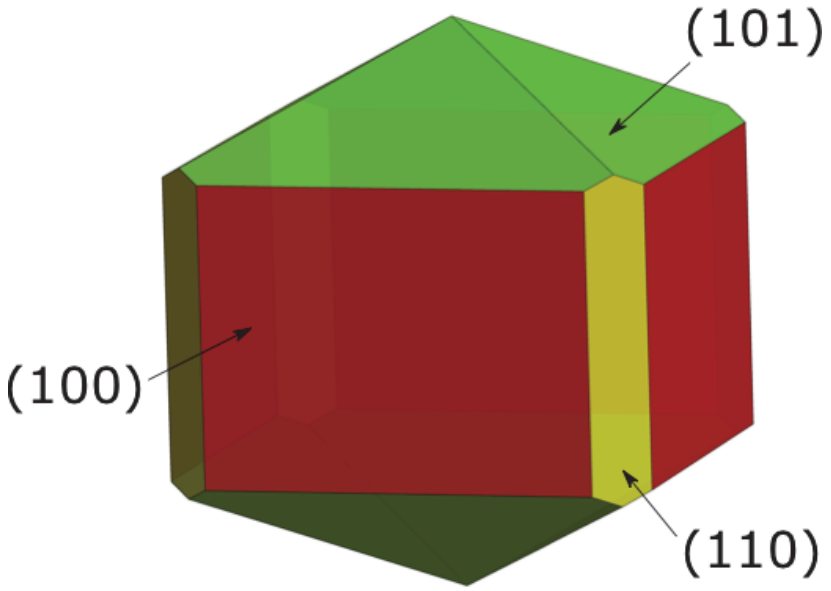

Figure 6. Equilibrium shape of β-Sn crystal from Wulff construction of calculated surface energies. (100) is the preferred surface. (001) does not manifest at all as a facet.

Table 1. Calculated surface energies (J/m^2) of Sn-based single crystals with different surface orientations. Calculations for O- (H, O-) terminated Sn are performed on tetragonal Sn with O (H and O) connected to the non-coordinated surface Sn atoms.

Material	(100)	(001)
β-Sn	0.39	0.49
O-terminated β-Sn	1.15	1.76
(H, O)-terminated β-Sn	3.08	5.01

Table 2. Calculated surface energies of β-Sn. Two different terminations of (101) surface for β-Sn are maked as a and b, respectively.

Miller index	Surface energy (J/m^2)
(100)	0.39
(001)	0.49
(101) a	0.41
(101) b	0.67
(110)	0.51
(111)	0.50

The impact of Sn crystal surface on the formation, composition and stability of the solid-electrolyte-interphases (SEIs) with the same electrolyte is revealed by soft x-ray absorption spectroscopy. SEI on the (100) surface is conventional porous Li_2CO_3 from electrolyte decomposition. In sharp contrast, a dense LiF layer dominates the SEI formed on the (001) surface from the decomposition of $LiPF_6$.

Keyword: Batteries

Ruimin Qiao, Ivan T. Lucas, Altaf Karim, Jaroslaw Syzdek, Xiaosong Liu, Wei Chen, Kristin Persson, Robert Kostecki, Wanli Yang*

Title: Distinct Solid-Electrolyte-Interphases on Sn (100) and (001) Electrodes Studied by Soft X-ray Spectroscopy

ToC figure